

3. METHODOLOGY

generate the profiles, but allows the refinement of all model parameters. [DIFFaX+ is available from the author (matteo.leoni@unitn.it) on request.]

3.6.2.6.8. Antiphase domain boundaries

In the diffraction pattern of an ordered alloy, a dissimilar broadening can often be observed for structure and superstructure peaks (with the former being present in both the ordered and disordered states). The superstructure peaks, in fact, bear microstructural information on the interface between the ordered regions in the material: broadening occurs when domains meet out of phase, creating an antiphase domain boundary (APB or APDB). A general formula for APDB-related broadening does not exist: for a given ordered structure, the Fourier coefficients correspond to the normalized value of $A_{APDB,hkl}(L) = \overline{F(0)F^*(L)}$, where $F(0)$ is the structure factor of a cell positioned at $L = 0$ and $F^*(L)$ is the complex conjugate of the structure factor of a cell at a distance L along the direction $[hkl]$. Being the result of a combination of probabilities, the peak is always expected to be Lorentzian.

Explicit formulae have been derived for the Cu₃Au ordered alloy (L₁₂ phase; Wilson, 1943; Wilson & Zsoldos, 1966; Scardi & Leoni, 2005). Several types of boundaries can form, depending on the way that the domains meet: the broadening depends both on the boundary plane and on the local arrangement of Au atoms leading to conservative (no Au atoms in contact) or nonconservative (Au atoms in contact) boundaries. By arranging the indices

in such a way that $h \geq k \geq l$ and that l is always the unpaired index, the broadening of the superstructure reflections can be described as (Scardi & Leoni, 2005)

$$A^{APDB}(L) = \exp[-2L\delta f(h, k, l)]. \tag{3.6.51}$$

In this formula, $\delta = \gamma_{APDB}/a_0$ is the probability of occurrence of an APDB, a_0 is the unit-cell parameter and $f(h, k, l)$ is a function of hkl defined in Table 3.6.2, obtained from the results of Wilson (1943) and Wilson & Zsoldos (1966).

The average distance between two APDBs is given by $1/\delta$. For a random distribution of faults, the broadening is Lorentzian and $A^{APDB} = \exp(-4L\delta/3)$.

3.6.2.7. Assembling the equations into a peak and modelling the data

As previously mentioned, the broadening contributions briefly illustrated in the previous sections are employed to generate the powder peak profile for reflections from the set of planes $\{hkl\}$ using equations (3.6.11) and (3.6.12) and where

$$\begin{aligned} I_{hkl}(s) &= k(d^*) \int_{-\infty}^{\infty} C(L) \exp(2\pi i L s) dL \\ &= k(s) \int_{-\infty}^{\infty} T_{pV}^{IP}(L) A_{hkl}^S(L) [A_{hkl}^D(L) \cos(2\pi L s) + i B_{hkl}^D(L) \sin(2\pi L s)] \\ &\quad \times \dots \times [A_{hkl}^F(L) \cos(2\pi L s) + i B_{hkl}^F(L) \sin(2\pi L s)] dL. \end{aligned} \tag{3.6.52}$$

Table 3.6.2

Models for antiphase domain boundaries for the Cu₃Au case

$$N = h^2 + k^2 + l^2.$$

ID	Model	$f(h, k, l)$
1	Random	2/3
2	{100} planes	$\frac{2h+k+l}{3\sqrt{N}}$
2.I	{100} planes, no Au–Au contacts	$(k+l)/\sqrt{N}$ if h is the unpaired index $(h+l)/\sqrt{N}$ if k is the unpaired index $(h+k)/\sqrt{N}$ if l is the unpaired index
2.II	{100} planes, only Au–Au contacts	$\frac{2h+k+l}{2\sqrt{N}}$ if h is the unpaired index $\frac{h+2k+l}{2\sqrt{N}}$ if k is the unpaired index $\frac{h+k+2l}{2\sqrt{N}}$ if l is the unpaired index
3	{110} planes	$\frac{2h+2k}{3\sqrt{2N}}$
3.I	{110} planes, Au displacement parallel or perpendicular to plane normal	$\frac{4h}{\sqrt{2N}}$ if h is the unpaired index $\frac{2h+2k}{\sqrt{2N}}$ otherwise
3.II	{110} planes, Au displacement at 60° to plane normal	$\frac{2h+2k}{\sqrt{2N}}$ if h is the unpaired index $\frac{3h+k}{\sqrt{2N}}$ otherwise
4	{111} planes	$\frac{8h}{3\sqrt{3N}}$ if $h \geq (k+l)$ $\frac{4(h+k+l)}{3\sqrt{3N}}$ otherwise

3.6. WHOLE POWDER PATTERN MODELLING

Equation (3.6.52) represents an asymmetrical peak profile (the asymmetry is given by the sine terms). Fast Fourier transform and space remapping (usually s to 2θ) are then employed to generate the peaks in the measurement space; intensities are multiplied by the Lorentz and, if needed, polarization terms, and a background is added to the whole pattern. Other aberrations (affecting the position, the intensity or the shape of the peak) can be included as needed.

The various reflections are then positioned on the basis of the (reference) Bragg angle $2\theta_B$ calculated from the unit-cell parameters, and a background (for example, a Chebychev polynomial) is suitably added. For completeness, thermal diffuse scattering should be included, as it can contribute to the broadening near the peak tails (see, for example, Beyerlein *et al.*, 2012). In addition, small-angle scattering can be considered to improve the WPPM result and to account for the observed increase in the background at low angle (Scardi *et al.*, 2011). The final equation is thus similar to that of the Rietveld (1969) or the Pawley (1981) methods,

$$I(2\theta) = \text{SAXS} + \text{TDS} + \text{bkg} + k(2\theta)LP \sum_{hkl} I_{\{hkl\}}(x), \quad (3.6.53)$$

the main difference being in the focus of the analysis and in the way that the profiles are generated.

The model parameters are then refined using a nonlinear least-squares routine (*e.g.* based on the Marquardt algorithm or suitable modifications, as proposed, for example, by Coelho, 2005) to directly match the synthesized pattern to the experimental data. The usual weight, related to Poisson counting statistics, is employed.

As the shape of each peak is bound to the underlying physical models, the number of parameters to be refined is usually quite limited. Compared with the four parameters per peak (intensity, width, shape and position) necessary for a Scherrer-type analysis, in WPPM we refine, for example, two parameters for a domain-size distribution, three parameters for dislocations (ρ , R'_e and φ), two parameters for faulting (α and β), at most six lattice parameters, a few background parameters (*e.g.* four parameters) and one parameter (intensity) per peak. In addition, we can also refine some further specimen-related parameters such as a misalignment error. No atomic coordinates are involved.

A flexible software package implementing WPPM (*PM2K*: Leoni *et al.*, 2006) is available from the author on request (matteo.leoni@unitn.it): the software includes all of the broadening models illustrated here. The user can work with any type and any simultaneous set of diffraction data (X-ray, neutrons or electrons) and build their own model with no *a priori* restriction on the quantity and type of parameters, the number of phases, the models or the relationships between the parameters. The WPPM method has also been implemented in the *TOPAS* refinement software [version 5 (Coelho, 2009; Bruker, 2009)] using the flexible macro language provided.¹

3.6.2.7.1. Alternative approaches

Convolutional multiple whole profile fitting (CMWP; Ribárik *et al.*, 2004) and extended convolutional multiple whole profile

fitting (eCMWP; Balogh *et al.*, 2006) have been developed to solve the same problem.

CMWP, introduced as a convolutive version of multiple whole profile fitting (MWP; Ungár *et al.*, 2001; Ribárik, 2008), is very similar to the WPPM. The notable differences are:

- (i) The instrumental profile is employed directly without interpolation and the profile of the instrumental peak closest to the peak under analysis is used. The instrumental profile imposes conditions on the range of L used in profile modelling.
- (ii) In CMWP a subset of data points is used for speed.
- (iii) The background is given by the user (as a spline or Legendre polynomial).
- (iv) All points of a given (generated) peak are weighted by the same value related to the maximum intensity. However, the correct weighting scheme with individual weights for data points is available as an option.

The authors also suggest using the MWP procedure in other cases, for example separately measured profiles or single crystals. The MWP procedure works in Fourier space so there is no direct possibility of checking the agreement between the model and data.

In the extended version (Balogh *et al.*, 2006), (e)CMWP introduces an interesting model for faults based on a parameterization of the profiles simulated with the *DIFFaX* software (Treacy *et al.*, 1991). This simulates the diffraction pattern of a faulted structure within the tangent cylinder approximation. The proposed parameterization allows more complex faulting models, at the expense of the calculation and parameterization of the profiles for any new, intermediate or mixed case or for any peak lying outside the parameterized range. The application of (e)CMWP is limited to cubic, hexagonal and orthorhombic powders with spherical or ellipsoidal domain shapes and assumes the presence of dislocations and faults.

It is worth mentioning two more alternative approaches: the Debye scattering equation (Debye, 1915; for some applications, see, for example, Cervellino *et al.*, 2003; Cozzoli *et al.*, 2006) and the total scattering (TS) approach [also known as pair distribution function (PDF) analysis; Egami & Billinge, 2003; Billinge, 2008; see also Chapter 5.7]. Both techniques work in real space: the first creates the pattern directly from atomic positions and the other extracts the real-space information (the PDF) from the diffraction data. As the information content does not change on moving from reciprocal (measured) to direct space, provided that similar hypotheses are employed (similar microstructure and, if necessary, structure), real-space and reciprocal-space methods should give similar results. Of course there are differences, related to the way that the data are handled. For instance, it is easier to visualize the anisotropic effects in reciprocal space, as the information is contained in the peak broadening (different peaks show different breadths): in the PDF this information is sparser as it should be reflected in a variation in the correlation lengths, but also (highly integrated) in a variation of the decay of the curve. Conversely, information on the atomic arrangement (*i.e.* on possible defects) appears more clearly in the PDF, where variations in the distances and in coordination are well localized, contrary to the diffraction pattern, where the information is contained in the (weak) diffuse signal, in the broadening and in the peak position.

Direct-space and reciprocal-space methods thus each have their own advantages and disadvantages. Combined or comparative modelling, whenever possible, is therefore always the best solution: we can match the flexibility and immediacy

¹Some small errors are present in some versions of the WPPM macros implemented in *TOPAS*. An example of a corrected macro for a lognormal distribution of spheres is given in the supporting information. The implementation using the mean and variance of the distribution *versus* the lognormal mean and variance is straightforward. Please refer to Chapter 5.1 for corrected versions of the Fourier coefficients and ancillary equations that should be present in the macros.

3. METHODOLOGY

of a real-space approach with the possibility of working directly with the measured data as typical in reciprocal-space methods.

3.6.3. Examples of WPPM analysis

To illustrate the power of the WPPM approach, a few examples are provided based both on simulated and on real data. The analyses were performed using the *PM2K* software (Leoni *et al.*, 2006). Similar results are obtained using the WPPM implementation in the commercial program *TOPAS*.

3.6.3.1. Nanocrystalline ceria

The first example concerns a nanocrystalline ceria powder obtained by the calcination of a cerium isopropoxide gel (Leoni, Di Maggio *et al.*, 2004; Leoni & Scardi, 2004; Scardi *et al.*, 2004). A large amount of XRD and transmission electron microscopy (TEM) data have been collected on the same system (and specimen), starting from the xerogel and following calcination (Scardi *et al.*, 2010). Fig. 3.6.1(a) shows the X-ray powder diffraction pattern of the gel calcined for 1 h at 673 K measured with Cu radiation (40 kV, 45 mA) on a Rigaku PMG/VH diffractometer.

The data were collected over the 2θ range 18–154° (with a step of 0.05°) with a counting time of 60 s per step: a wide angular range and a high signal-to-noise ratio (SNR) are prerequisites for a proper line-profile analysis. The large span in reciprocal space is important for the complete characterization of any anisotropy in the broadening (a large set of independent directions in reciprocal space needs to be sampled), whereas the high SNR guarantees the collection of data at peak tails where the differences between similar microstructure models manifest themselves. The log scale employed in Fig. 3.6.1(a) highlights the low level of noise present in the pattern.

The diffractometer had 0.5° divergence and 2° Soller slits mounted on the primary arm and 0.15 mm antiscatter, 0.5° receiving and 2° Soller slits and a curved graphite analyzer crystal mounted on the secondary arm. This setup provided a narrow and symmetrical instrumental profile that could be described by a pseudo-Voigt curve and was thus ideal for line-profile analysis studies. The Caglioti *et al.* (1958) parameterization of the instrumental profile [*cf.* equations (3.6.18) and (3.6.19)] performed on the profiles of the NIST SRM 660a standard (LaB₆) is shown in Fig. 3.6.2.

Analysis of the pattern using traditional methods (see Scardi *et al.*, 2004) required 59 parameters, 53 of which were actually refined:

- (i) one unit-cell parameter (a_0),
- (ii) six (fixed) parameters defining the instrumental contribution [five parameters for the Caglioti parameterization (U , V , W , a and b) and one for the $K\alpha_2$ intensity ratio],
- (iii) three parameters for the background,
- (iv) one parameter for the specimen displacement,
- (v) 48 parameters for the peaks (intensity, FWHM and shape for 16 peaks).

An analysis using traditional analysis methods resulted in an ‘average domain size’ of 3.65 (10) nm using the (modified) Warren–Averbach method and in the range from 4.95 (10) to 5.3 (1) nm using a (modified) Williamson–Hall approach. A discussion of the meaning and accuracy of the results can be found in Scardi *et al.* (2004).

The WPPM result, shown in Fig. 3.6.1(b), matches the experiment quite well: this is remarkable considering that the

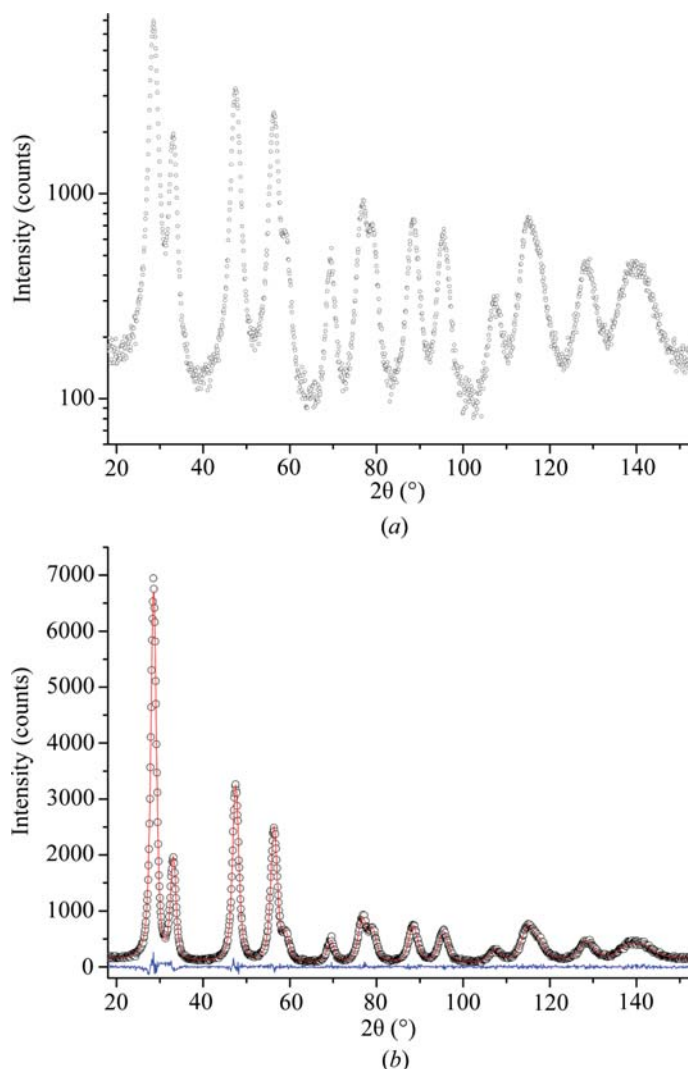


Figure 3.6.1

X-ray powder diffraction pattern of nanocrystalline ceria calcined at 673 K. In (a) the pattern is shown on a log scale to highlight the weak features in the data. In (b) the results of WPPM are shown: raw data (dots), model (line) and difference (lower line).

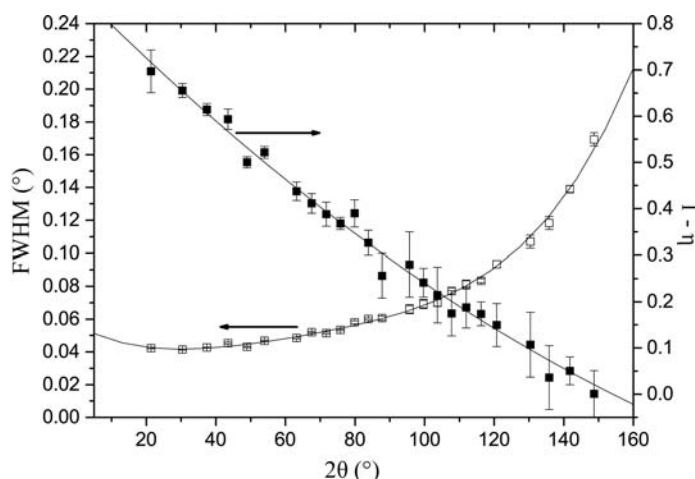


Figure 3.6.2

Parameterization of the instrumental resolution function using a pseudo-Voigt and the relationship of Caglioti *et al.* (1958).

whole pattern (1800 data points) is modelled using just 32 parameters (26 free parameters):

- (i) one unit-cell parameter (a_0),
- (ii) six (fixed) parameters defining the instrumental contribution [five parameters for the Caglioti parameterization (U , V , W , a and b) and one for the $K\alpha_2$ intensity ratio],